Tailoring Temperature Coefficient of Resistance of

Silver Nanowire Nanocomposite and Application as

Stretchable Temperature Sensor

Zheng Cui, Felipe Robles Poblete, Yong Zhu*

Department of Mechanical and Aerospace Engineering, North Carolina State University,

Raleigh, NC 27606, USA

Keywords: silver nanowire, stretchable, wearable, breathable, kirigami

ABSTRACT: Body temperature is an important indicator of health condition. It is of critical

importance to develop smart temperature sensor for wearable applications. Silver nanowire

(AgNW) is a promising conductive material for developing flexible and stretchable electrodes.

Here, a stretchable thermoresistive temperature sensor based on AgNW composite is developed,

where AgNW percolation network is encased in a thin polyimide film. Temperature coefficient

of resistance (TCR) of the AgNW network is tailored by modifying nanowire density and

thermal annealing temperature. The temperature sensor is patterned with a Kirigami structure,

which enables constant resistance under a large tensile strain (up to 100%). Demonstrated

applications in monitoring the temperatures at biceps and knees using the stretchable temperature

sensor illustrate the promising potential for wearable applications.

1

INTRODUCTION

Highly sensitive flexible and stretchable sensors that can be used to monitor vital biosignal, such as body temperature, ¹⁻⁴ respiration rate, ⁵⁻⁶ blood pressure, ⁷⁻⁸ glucose level, ⁹ and electrophysiology signals, ¹⁰⁻¹¹ have garnered tremendous interest. Such devices can be conformally attached to human skin or integrated with textiles to realize its functionality. Body temperature is one of the most important biosignals, which is closely associated with a variety of illnesses/diseases, e.g., acute stroke, ¹² sleep quality, ¹³ osteoarthritis pain, ¹⁴⁻¹⁵ and breast cancer. ¹⁶ Additionally, high body temperature speeds up the fatigue in trainers during prolonged exercises. ¹⁷⁻¹⁸ In order to realize long-term monitoring of body temperature, the temperature sensor should be flexible and stretchable in order to be conformally attached to human skin. In particular, the sensor needs to be stretchable to accommodate large strain when attached to areas such as muscles and joints. ¹⁹ Moreover, the temperature sensor should be vapor-permeable to prevent heat and sweat accumulation that causes discomfort.

Thermoresistive effect is typically used for temperature sensing. The resistance of a conductive material changes with temperature due to thermally introduced charge carrier scattering (resistance increase) or thermally enhanced charge transport (resistance decrease). Several stretchable temperature sensors based on the thermoresistive effect have been developed using thin film metals, 1, 19, 21 graphene, 22-23 and carbon nanotubes (CNTs), 2, 24-25 and metallic nanowires. However, most of the stretchable sensors suffer crosstalk between temperature and strain as resistance change can be caused by either temperature change or applied strain. 22-23, 26-27

Bulk Ag has a high temperature coefficient of resistance (TCR) of 3.8×10-3)/°C at 20 °C, which is close to the widely used material for temperature sensor, Pt (3.9×10-3/°C). Ag nanowire (AgNW) is a promising conductive material that has been widely used in flexible and stretchable devices. Wang et al. found that a single AgNW exhibits higher TCR than that of bulk Ag.²⁸ Hence, AgNW can be potentially an excellent candidate for flexible and stretchable temperature sensor.

Here, we report a breathable, stretchable but strain-insensitive temperature sensor based on a composite material consisting of AgNW network and polyimide (PI) matrix. TCR of the AgNW network was characterized in the temperature range from 25 to 60 °C, of relevance to wearable applications. TCR was found to depend on AgNW density and annealing temperature, that is, TCR increases with increasing AgNW density and increasing annealing temperature. However, it is known that resistance of the AgNW composite depends on the applied strain too. To achieve large stretchability for wearable applications and at the same time true temperature sensing that is insensitive to strain, a Kirigami-inspired structure was adopted. As a result, the temperature sensor can be used under a large strain (up to 100%) but with no crosstalk from the applied strain. The temperature sensor was used to monitor the skin temperature at biceps and knees under motion, demonstrating outstanding performances of the sensor for wearable applications.

RESULTS AND DISCUSSION

Fabrication process of the stretchable temperature sensor is shown in Figure 1. (i) AgNW ink was spray-coated on a pre-cleaned glass slide to form a AgNW percolation network;²⁹⁻³⁰ (ii) Then the AgNW network was thermally annealed to reduce the contact resistance between AgNWs; (iii) A thin layer of PI resin was spin-coated on the AgNW film, followed by curing;

(iv) The cured AgNW/PI thin film was patterned into the designed Kirigami pattern by laser cutting; (v) Finally, the patterned AgNW/PI was peeled from the glass substrate by a water-assisted method.³¹ Thin copper wires were attached at the two ends of the AgNW/PI film as lead wires using Ag paste. The AgNWs were inlaid into the surface layer of the PI film as shown in the SEM image (Figure 1f), forming a conductive surface. Compared to AgNWs on top of a film, this inlaid type of structure is mechanically robust and wear resistant.

AgNW density and annealing temperature have important effects on TCR of the AgNW films. To identify the optimal AgNW density and annealing temperature, AgNW networks on the glass slides were prepared. AgNWs were spray coated on the glass slide, following step (i) in Figure 1a, with different NW densities. Here the NW density is areal density, calculated from optical images, ranging from 0.26 to 2.05 nanowires per μm². The same AgNW networks were thermally annealed in a furnace (TF55035A-1) at 150 °C for 30 min and then at 200 °C for 30 min. Sheet resistance was measured following each annealing step. Figure 2a shows that thermal annealing decreased the sheet resistance of the AgNW network. This is because thermal annealing improves the contact between NWs by welding the NW junctions. Hence, the contact resistance in the nanowire network decreases and the AgNW network becomes more conductive. Moreover, the resistance change also depends on the NW density. For instance, for the lowest NW density (0.26 per μ m²), the sheet resistance decreased from 23.73 Ω sq⁻¹ to 11.38 Ω sq⁻¹ and $3.73 \Omega \text{ sq}^{-1}$ after annealing at 150 °C and 200 °C, respectively; while for the highest NW density (2.05 per μ m²), it did from 0.73 Ω sq⁻¹ to 0.64 Ω sq⁻¹ and 0.55 Ω sq⁻¹, respectively. SEM images of the AgNW junctions after thermal annealing at different temperatures are shown in Figure 2b. It can be seen that higher annealing temperature leads to better contact between the AgNWs.

TCR of the AgNW network was extracted from the resistance vs. temperature data. Thermoresistive behaviors of the AgNW network (at density of 2.053 per μ m²) at three thermal annealing conditions (as-prepared, after 150 °C annealing, and after 200 °C annealing) are shown in Figure 2c as an example. More thermoresistive behaviors at other NW densities are shown in Figure S1, Supporting Information. The resistance change showed excellent linearity in the temperature range tested (25 – 60 °C). TCR of the AgNW network, which is defined as follows, can be extracted from the thermoresistive curve,

$$TCR = \frac{1}{R(T_0)} \frac{R(T) - R(T_0)}{T - T_0} \tag{1}$$

where R(T₀) is the resistance at T₀ (usually room temperature, here taken as 25 °C) and R(T) is the resistance at T. TCRs of the five AgNW networks at different densities were calculated with and without the annealing, as plotted in Figure 2d together with the TCR of bulk Ag (3.8×10⁻³/°C). It was found that AgNW network with higher NW density has a higher TCR. Before thermal annealing, the AgNW networks with densities of 0.263 and 2.053 per μm² showed TCRs of 2.62×10⁻³/°C and 2.94×10⁻³/°C, respectively. It was also found that thermal annealing can increase the TCR of the AgNW network. For instance, for the AgNW network with density of 2.053 per μm², TCR increased from 2.94×10⁻³/°C as prepared to 3.24×10⁻³/°C and 3.32×10⁻³/°C after thermal annealing at 150 °C and 200 °C, respectively. These observations can be understood by comparing AgNW network and Ag thin film. AgNW network with higher density behaves more like a thin Ag film. After annealing, the contacts between AgNWs are annealed and the polymer coatings around the NWs (e.g., polyvinylpyrrolidone formed during the AgNW synthesis) are partially removed, so the AgNWs are transformed from a discrete structure (i.e. percolation network) to a more continuous structure, similar to a thin Ag film. Due to the voids

(open space) in the NW network and residue polymer coatings, TCRs of the AgNW networks are lower than that of bulk Ag.

In addition to the sheet resistance and TCR measurements, optical transmittances of the AgNW networks were measured, as shown in Figure S2, Supporting Information. All these measurement results can provide valuable information for selecting the optimal materials for the desired temperature sensors. In this work, we selected the AgNW network with the largest density (2.053 per μ m²) after 200 °C thermal annealing in order to achieve the largest TCR. However, different densities and annealing conditions could be used to meet different needs. For example, if a transparent temperature sensor is desired, the AgNW network with a lower density should be used.

To fabricate the temperature sensor, we further processed the selected AgNW network following steps (iii) to (v) as shown in Figure 1. Of course one question arises whether the AgNW network on glass substrate and the same AgNW network but embedded in PI have the same TCR, which will be addressed later. Kirigami, in which cuts are introduced into a 2D sheet, can transform the non-stretchable 2D sheet into a highly stretchable 3D structure. As a result, Kirigami pattern can accommodate large applied tensile strain by out-of-plane deformation, minimizing the local strain in the sheet. Moreover, the cuts in the Kirigami structure make the thin film breathable, improving the comfort of long-term wear. Recently, the kirigami-inspired approach has been applied to develop ultra-stretchable devices. 32-36 In this work, the designed Kirigami pattern had an array of straight, parallel cut lines (Figure 3a), with the slit length of 6 mm, slit gap of 2 mm, and beam width of 1 mm. To avoid stress concentration at the ends of the slits (i.e. crack tips), the ends were rounded with a radius of 0.2 mm. Detailed geometry design can be found in Figure S3, Supporting Information.

The strain sensitivity of the fabricated AgNW/PI temperature sensor was characterized. Thermoplastic polyurethane (TPU) was used to attach the two ends of the AgNW/PI sensor on a stretchable substrate by heat pressing. Then the sample was installed on a customized tensile stage, as shown in Figure 3a. Tensile testing was carried out while the resistance of the AgNW/PI sensor was measured simultaneously. The sensor showed outstanding resistance stability under tensile testing up to 100% strain. The variation of the resistance was within 0.05%, which was attributed to the Kirigami pattern that effectively released the local strain applied on the AgNW network. FEA simulations using Abaqus were carried out and agreed well with the experiments in terms of the deformed morphology (Figures 3a, b). FEA simulations showed the average tensile strain of 0.03% (with the maximum strain of 0.56%) in the loading direction, when the applied strain was 100%. Gage factor of metals is given by 1+2v, where v is the Poisson's ratio. Considering that the gage factor of Ag is 1.74 (v = 0.37), the 0.05% resistance change correlates well with the 0.03% average strain. The FEA simulations also confirmed that out-of-plane deformation is effective in reducing the local strain. Cyclic loading of 100% strain was conducted at 1 Hz and the result showed stable resistance for more than 1000 cycles (Figure 3c).

The performance of the AgNW/PI film as a stretchable temperature sensor was evaluated at the temperature range of 25 °C to 60 °C on a hot plate. A thermocouple was used to calibrate the temperature on the AgNW/PI film. The resistance of the sensor was measured under 0 % and 100 % strain. The measured resistance change $\Delta R/R0$ as a function of the measured temperature of the sensor is plotted for both strains in Figure 3d, again showing nearly no difference, consistent with the results shown in Figure 3c. The calculated TCR of the AgNW/PI film was 3.32×10^{-3} °C, and the sensitivity of the temperature sensor was 0.47Ω °C (the initial resistance

of the sensor was 145 Ω). With introduction of the Kirigami cuts, the resistance increased significantly (c.f., the values shown in Figure 2c). To achieve high sensitivity, it is important for the temperature sensor to have much larger resistance than that of the lead wires or metal interconnects because the lead wires/interconnects also have the TCR function. Note that for the same AgNW network with the density of 2.053 per μ m² after 200 °C annealing exhibited the same TCR, either on top of the glass substrate or embedded in the PI film. The sensing performance and stretchability in this work is listed in Table 1, along with previously reported thermoresistive temperature sensors, for the purpose of comparison.

The temperature sensor was applied to human body to demonstrate its general capabilities for wearable applications. Muscle temperature is a key factor during workout. Muscle temperature increases due to the metabolism during intense, dynamic exercises. Higher temperature can cause increased fatigue and possible injuries. ¹⁷ Our temperature sensor was attached to the biceps of a male subject to monitor the local temperatures on skin, as shown in Figure 4a. Skin temperature was recorded while the subject was lifting a dumbbell, in which large skin deformation was introduced to the biceps. Our sensor is only 9 µm in thickness, which leads to conformal contact with the skin. Hence, the sensor temperature is essentially the same as the temperature of the skin surface. A commercially available infrared thermometer (ANKOVO) was used to monitor the temperature at the targeted area simultaneously. The temperatures recorded from the AgNW/PI temperature sensor and infrared thermometer are plotted in Figure 4b. The skin temperature of the subject's biceps was 35.3 °C before the workout, and increased up to 36.8 °C during the workout. The temperature recorded by IR thermometer before and during the workout were 35.2 °C and 36.7 °C, respectively.

Osteoarthritis is the most common chronic condition of the joints, affecting millions of people worldwide. It has been shown that patellar skin surface temperature can be used to monitor the severity of knee osteoarthritis. The temperature sensor was attached to the knee of a male subject, as shown in Figure 4c. Skin temperature was recorded by both the sensors and the infrared thermometer simultaneously while the subject was doing squad. The skin temperature at the subject's knee during the squad workout was relative stable due to thin fat and muscle layer at the knee. The average temperatures recorded by the temperature sensor and infrared thermometer were 25.1 °C and 29.0 °C, respectively. The two demonstrations above illustrated that the AgNW/PI temperature sensor can monitor the subtle skin temperature change during large body deformation.

CONCLUSION

In summary, we report a Kirigami-inspired breathable and stretchable temperature sensor based on AgNWs for wearable applications. The sensing mechanism is based on thermoresistive effect of AgNW network embedded in PI film. TCRs of AgNW networks with different NW densities were measured. Higher AgNW density resulted in a higher TCR. Thermal annealing was found to enhance the TCR of NW films by improving the contact between NWs and removing the polymer coating around the NWs. AgNW network with the density of 2.053 per μ m² after 200 °C annealing was selected to fabricate the temperature sensor, with the TCR of 3.32×10^{-3} °C and the sensitivity of 0.47 Ω /°C. With the designed Kirigami pattern, local strain was effectively minimized due to the out-of-plane deformation when a large tensile strain was applied. Cyclic tensile testing at 100% strain was carried out, exhibiting stable resistance over 1000 cycles. Skin temperatures at biceps and knee were monitored, illustrating the general capabilities of the AgNW-based stretchable temperature sensor for wearable applications.

EXPERIMENT SECTION

AgNW ink preparation: AgNW was synthesized by the polyol method. The as-synthesized AgNW has an average diameter of 120 nm and an average length of \sim 25 μ m. AgNW was diluted in ethanol with a concentration of 1 mg/ml for the spray coating.

AgNW deposition: An airbrush (A4709, Aztek) was used to deposit the NWs on pre-cleaned glass slides (0215 glass, Corning). The AgNW ink was spray-coated with a back pressure of 10 psi (Iwata studio series air compressor) and nozzle-substrate distance of ~15 cm. The glass slides were placed on top of a hot plate during the coating process to speed up the evaporation of AgNW solvent.

PI resin coating: Colorless PI resin (CP1 polyimide resin, NeXolve) was spin-coated on the AgNW network at 500 rpm for 30 sec. Then the resin was cured at 60 °C for 3 hrs. The thickness of the AgNW/PI film was ~9 μm as measured by Ellipsometer (P-7 profilometer, KLA-Tencor).

Laser cutting and packaging: The AgNW/PI film was cut into the designed Kirigami pattern by a laser cutter (VLS6.60, Universal Laser Systems). The cutting parameters include 0.8% power, 50% speed, and 1000 PPI in Raster mode. With this setting, the width of the laser-cut trace in AgNW/PI film is ~270 μm. After laser cutting, the AgNW/PI film was released from the glass slide by soaking it in DI water. And then the sample was transferred onto a glass slide with the AgNW side faces up. Copper wires were bonded to the AgNW as the lead wires.

TCR characterization: Performances of the AgNW/PI temperature sensors were characterized on a hot plate. A thermocouple thermometer (HH802U, Omega) was used to obtain the local temperature on the temperature sensor and a digital multimeter (34401A, Agilent) was used to monitor the resistance of the sensor by 4W measurement.

Stretchability characterization: The AgNW/PI temperature sensor was attached onto a

stretchable substrate with TPU film by heat press. Then the sample was mounted on a custom-

made testing stage for tensile testing.

ASSOCIATED CONTENT

Supporting Information.

The following files are available free of charge.

More data of resistance vs. temperature for samples with different NW concentrations,

transmittance of NW networks with different concentration, details of kirigami structure design,

details of finite element analysis of the kirigami structure. (Figure S1-S3)

AUTHOR INFORMATION

Corresponding Author

*E-mail: yong zhu@ncsu.edu (Y. Z.).

Author Contributions

The manuscript was written through contributions of all authors. All authors have given approval

to the final version of the manuscript.

ACKNOWLEDGMENT

The work was supported in part by the National Science Foundation (NSF) through Awards

Nos. IIS-1637892 and CMMI-1728370. ZC would like to thank Nrup Balar and Ronald Booth

for their help with profilometer measurement and Hongyu Wang for SEM imaging.

11

REFERENCES

- 1. Fan, J. A.; Yeo, W.-H.; Su, Y.; Hattori, Y.; Lee, W.; Jung, S.-Y.; Zhang, Y.; Liu, Z.; Cheng, H.; Falgout, L.; Bajema, M.; Coleman, T.; Gregoire, D.; Larsen, R. J.; Huang, Y.; Rogers, J. A., Fractal Design Concepts for Stretchable Electronics. *Nat. Commun.* **2014**, *5*, 3266.
- 2. Honda, W.; Harada, S.; Arie, T.; Akita, S.; Takei, K., Wearable, Human-Interactive, Health-Monitoring, Wireless Devices Fabricated by Macroscale Printing Techniques. *Adv. Funct. Mater.* **2014,** *24* (22), 3299-3304.
- 3. Chen, Y.; Lu, B.; Chen, Y.; Feng, X., Breathable and Stretchable Temperature Sensors Inspired by Skin. *Sci. Rep.* **2015**, *5*, 11505.
- 4. Trung, T. Q.; Ramasundaram, S.; Hwang, B. U.; Lee, N. E., An All-Elastomeric Transparent and Stretchable Temperature Sensor for Body-Attachable Wearable Electronics. *Adv. Mater.* **2016**, *28* (3), 502-509.
- 5. Hwang, B.-U.; Lee, J.-H.; Trung, T. Q.; Roh, E.; Kim, D.-I.; Kim, S.-W.; Lee, N.-E., Transparent Stretchable Self-Powered Patchable Sensor Platform with Ultrasensitive Recognition of Human Activities. *ACS Nano* **2015**, *9* (9), 8801-8810.
- 6. Bai, P.; Zhu, G.; Jing, Q.; Yang, J.; Chen, J.; Su, Y.; Ma, J.; Zhang, G.; Wang, Z. L., Membrane-Based Self-Powered Triboelectric Sensors for Pressure Change Detection and Its Uses in Security Surveillance and Healthcare Monitoring. *Adv. Funct. Mater.* **2014**, *24* (37), 5807-5813.
- 7. Gong, S.; Schwalb, W.; Wang, Y.; Chen, Y.; Tang, Y.; Si, J.; Shirinzadeh, B.; Cheng, W., A Wearable and Highly Sensitive Pressure Sensor with Ultrathin Gold Nanowires. *Nat. Commun.* **2014**, *5*, 3132.

- 8. Luo, N.; Dai, W.; Li, C.; Zhou, Z.; Lu, L.; Poon, C. C.; Chen, S. C.; Zhang, Y.; Zhao, N., Flexible Piezoresistive Sensor Patch Enabling Ultralow Power Cuffless Blood Pressure Measurement. *Adv. Funct. Mater.* **2016**, *26* (8), 1178-1187.
- 9. Bandodkar, A. J.; Jeerapan, I.; You, J.-M.; Nuñez-Flores, R.; Wang, J., Highly Stretchable Fully-Printed Cnt-Based Electrochemical Sensors and Biofuel Cells: Combining Intrinsic and Design-Induced Stretchability. *Nano Lett.* **2015**, *16* (1), 721-727.
- 10. Myers, A. C.; Huang, H.; Zhu, Y., Wearable Silver Nanowire Dry Electrodes for Electrophysiological Sensing. *RSC Adv.* **2015**, *5* (15), 11627-11632.
- 11. Kim, D.-H.; Lu, N.; Ma, R.; Kim, Y.-S.; Kim, R.-H.; Wang, S.; Wu, J.; Won, S. M.; Tao, H.; Islam, A.; Yu, K. J.; Kim, T.-i.; Chowdhury, R.; Ying, M.; Xu, L.; Li, M.; Chung, H.-J.; Keum, H.; McCormick, M.; Liu, P.; Zhang, Y.-W.; Omenetto, F. G.; Huang, Y.; Coleman, T.; Rogers, J. A., Epidermal Electronics. *Science* **2011**, *333* (6044), 838-843.
- 12. Reith, J.; Jorgensen, H. S.; Pedersen, P. M.; Nakamaya, H.; Jeppesen, L.; Olsen, T.; Raaschou, H., Body Temperature in Acute Stroke: Relation to Stroke Severity, Infarct Size, Mortality, and Outcome. *Lancet* **1996**, *347* (8999), 422-425.
- 13. Campbell, S. S.; Gillin, J. C.; Kripke, D. F.; Erikson, P.; Clopton, P., Gender Differences in the Circadian Temperature Rhythms of Healthy Elderly Subjects: Relationships to Sleep Quality. *Sleep* **1989**, *12* (6), 529-536.
- 14. McAlindon, T.; Formica, M.; Schmid, C. H.; Fletcher, J., Changes in Barometric Pressure and Ambient Temperature Influence Osteoarthritis Pain. *Am. J. Med.* **2007**, *120* (5), 429-434.
- 15. Denoble, A. E.; Hall, N.; Pieper, C. F.; Kraus, V. B., Patellar Skin Surface Temperature by Thermography Reflects Knee Osteoarthritis Severity. *Clin. Med. Insights Arthritis Musculoskelet Disord.* **2010**, *3*, CMAMD-S5916.

- 16. Lawson, R., Implications of Surface Temperatures in the Diagnosis of Breast Cancer. *Can. Med. Assoc. J.* **1956,** *75* (4), 309.
- 17. González-Alonso, J.; Teller, C.; Andersen, S. L.; Jensen, F. B.; Hyldig, T.; Nielsen, B., Influence of Body Temperature on the Development of Fatigue During Prolonged Exercise in the Heat. *J. Appl. Physiol.* **1999**, *86* (3), 1032-1039.
- 18. MacDougall, J. D.; Reddan, W.; Layton, C.; Dempsey, J., Effects of Metabolic Hyperthermia on Performance During Heavy Prolonged Exercise. *J. Appl. Physiol.* **1974,** *36* (5), 538-544.
- 19. Webb, R. C.; Bonifas, A. P.; Behnaz, A.; Zhang, Y.; Yu, K. J.; Cheng, H.; Shi, M.; Bian, Z.; Liu, Z.; Kim, Y.-S.; Yeo, W.-H.; Park, J. S.; Song, J.; Li, Y.; Huang, Y.; Gorbach, A. M.; Rogers, J. A., Ultrathin Conformal Devices for Precise and Continuous Thermal Characterization of Human Skin. *Nat. Mater.* **2013**, *12* (10), 938.
- 20. Yao, S.; Swetha, P.; Zhu, Y., Nanomaterial-Enabled Wearable Sensors for Healthcare. *Adv. Healthc. Mater.* **2018,** *7* (1), 1700889.
- 21. Yu, C.; Wang, Z.; Yu, H.; Jiang, H., A Stretchable Temperature Sensor Based on Elastically Buckled Thin Film Devices on Elastomeric Substrates. *Appl. Phys. Lett.* **2009**, *95* (14), 141912.
- 22. Yang, J.; Wei, D.; Tang, L.; Song, X.; Luo, W.; Chu, J.; Gao, T.; Shi, H.; Du, C., Wearable Temperature Sensor Based on Graphene Nanowalls. *RSC Adv.* **2015**, *5* (32), 25609-25615.
- 23. Yan, C.; Wang, J.; Lee, P. S., Stretchable Graphene Thermistor with Tunable Thermal Index. *ACS Nano* **2015**, *9* (2), 2130-2137.

- 24. Harada, S.; Kanao, K.; Yamamoto, Y.; Arie, T.; Akita, S.; Takei, K., Fully Printed Flexible Fingerprint-Like Three-Axis Tactile and Slip Force and Temperature Sensors for Artificial Skin. *ACS Nano* **2014**, *8* (12), 12851-12857.
- 25. Hong, S. Y.; Lee, Y. H.; Park, H.; Jin, S. W.; Jeong, Y. R.; Yun, J.; You, I.; Zi, G.; Ha, J. S., Stretchable Active Matrix Temperature Sensor Array of Polyaniline Nanofibers for Electronic Skin. *Adv. Mater.* **2016**, *28* (5), 930-935.
- 26. Han, S.; Kim, M. K.; Wang, B.; Wie, D. S.; Wang, S.; Lee, C. H., Mechanically Reinforced Skin-Electronics with Networked Nanocomposite Elastomer. *Adv. Mater.* **2016**, *28* (46), 10257-10265.
- 27. Liao, X.; Liao, Q.; Zhang, Z.; Yan, X.; Liang, Q.; Wang, Q.; Li, M.; Zhang, Y., A Highly Stretchable Zno@ Fiber-Based Multifunctional Nanosensor for Strain/Temperature/Uv Detection. *Adv. Funct. Mater.* **2016**, *26* (18), 3074-3081.
- 28. Cheng, Z.; Liu, L.; Xu, S.; Lu, M.; Wang, X., Temperature Dependence of Electrical and Thermal Conduction in Single Silver Nanowire. *Sci. Rep.* **2015**, *5*, 10718.
- 29. Xu, F.; Zhu, Y., Highly Conductive and Stretchable Silver Nanowire Conductors. *Adv. Mater.* **2012**, *24* (37), 5117-5122.
- 30. Song, L.; Myers, A. C.; Adams, J. J.; Zhu, Y., Stretchable and Reversibly Deformable Radio Frequency Antennas Based on Silver Nanowires. *ACS Appl. Mater. Interfaces* **2014**, *6* (6), 4248-4253.
- 31. Gurarslan, A.; Yu, Y.; Su, L.; Yu, Y.; Suarez, F.; Yao, S.; Zhu, Y.; Ozturk, M.; Zhang, Y.; Cao, L., Surface-Energy-Assisted Perfect Transfer of Centimeter-Scale Monolayer and Few-Layer Mos2 Films onto Arbitrary Substrates. *ACS Nano* **2014**, *8* (11), 11522-11528.

- 32. Shyu, T. C.; Damasceno, P. F.; Dodd, P. M.; Lamoureux, A.; Xu, L.; Shlian, M.; Shtein, M.; Glotzer, S. C.; Kotov, N. A., A Kirigami Approach to Engineering Elasticity in Nanocomposites through Patterned Defects. *Nat. Mater.* **2015**, *14* (8), 785.
- 33. Song, Z.; Wang, X.; Lv, C.; An, Y.; Liang, M.; Ma, T.; He, D.; Zheng, Y.-J.; Huang, S.-Q.; Yu, H.; Jiang, H., Kirigami-Based Stretchable Lithium-Ion Batteries. *Sci. Rep.* **2015**, *5*, 10988.
- 34. Morikawa, Y.; Yamagiwa, S.; Sawahata, H.; Numano, R.; Koida, K.; Ishida, M.; Kawano, T., Ultrastretchable Kirigami Bioprobes. *Adv. Healthc. Mater.* **2018**, *7* (3), 1701100.
- 35. Lee, W.; Liu, Y.; Lee, Y.; Sharma, B. K.; Shinde, S. M.; Kim, S. D.; Nan, K.; Yan, Z.; Han, M.; Huang, Y.; Zhang, Y.; Ahn, J.-H.; Rogers, J., Two-Dimensional Materials in Functional Three-Dimensional Architectures with Applications in Photodetection and Imaging. *Nat. Commun.* **2018**, *9* (1), 1417.
- 36. Guan, Y. S.; Zhang, Z.; Tang, Y.; Yin, J.; Ren, S., Kirigami-Inspired Nanoconfined Polymer Conducting Nanosheets with 2000% Stretchability. *Adv. Mater.* **2018**, *30* (20), 1706390.

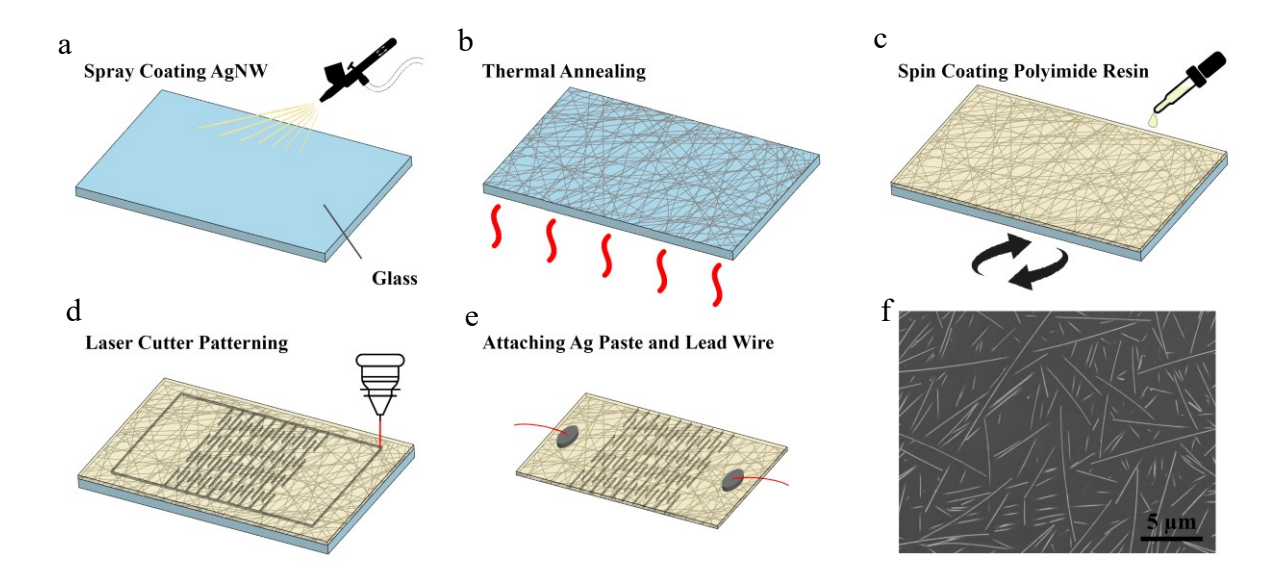


Figure 1 Fabrication process of AgNW/PI temperature sensor. a) AgNWs are spray-coated on glass slide. b) AgNW network on glass slide is thermally annealed. c) Colorless polyimide resin is spin-coated on the AgNW network and cured. d) Cured AgNW/PI film is patterned in a Kirigami structure by laser cutting. e) Attach lead wires. f) SEM image of the AgNW/PI composite with the AgNW side exposed. Scale bar, 5 μm.

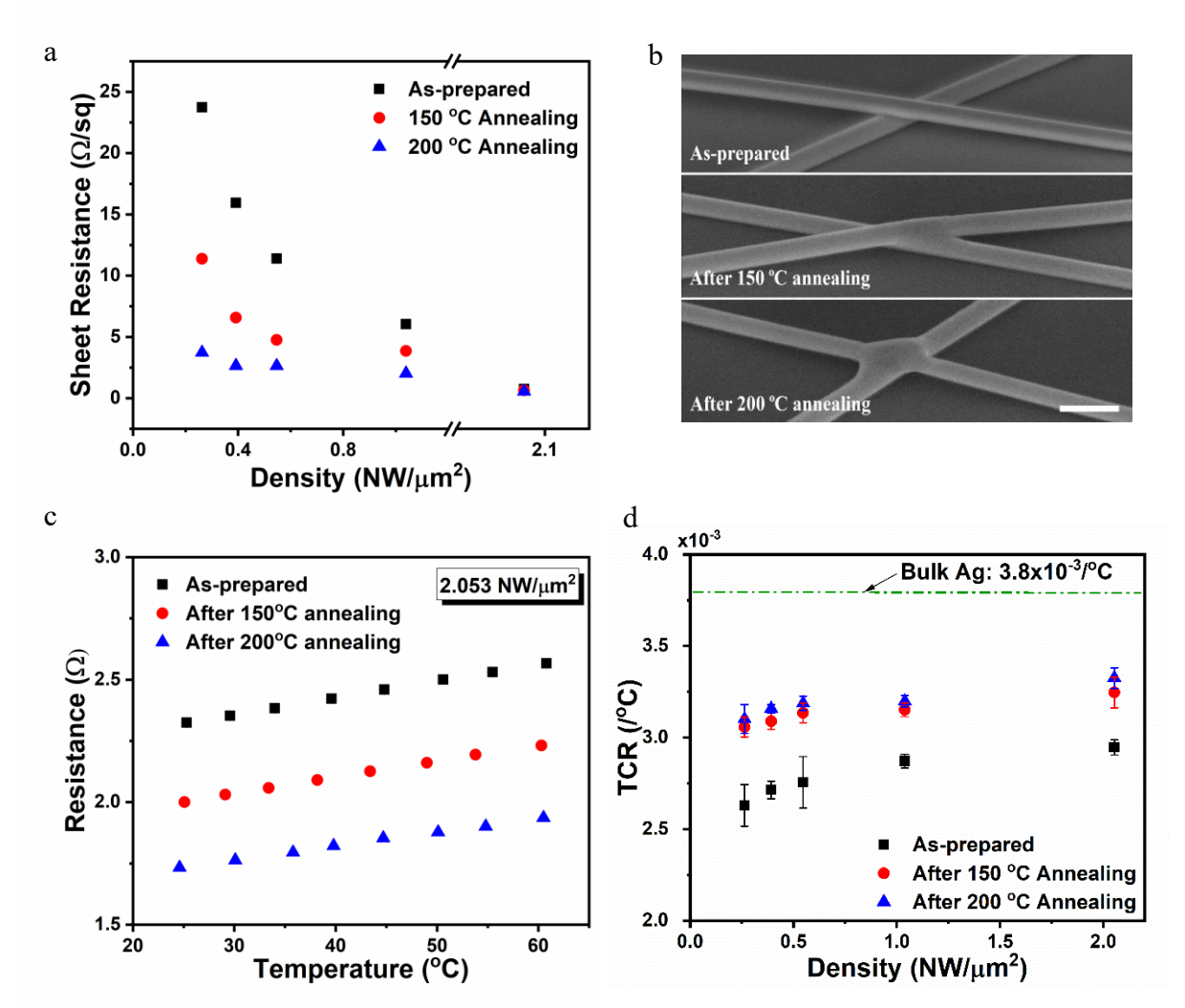


Figure 2 a) Sheet resistance vs. AgNW density at three thermal annealing conditions: asprepared, after 150 °C annealing, and after 200 °C annealing. b) SEM images showing AgNW junctions at the three annealing conditions. Scale bar: 200 nm. c) Thermoelectric behavior of the AgNW network with nanowire density of 2.05 NW/μm² at the three annealing conditions. d) TCR of AgNW networks with different nanowire densities at the three annealing conditions. TCR of bulk Ag is included.

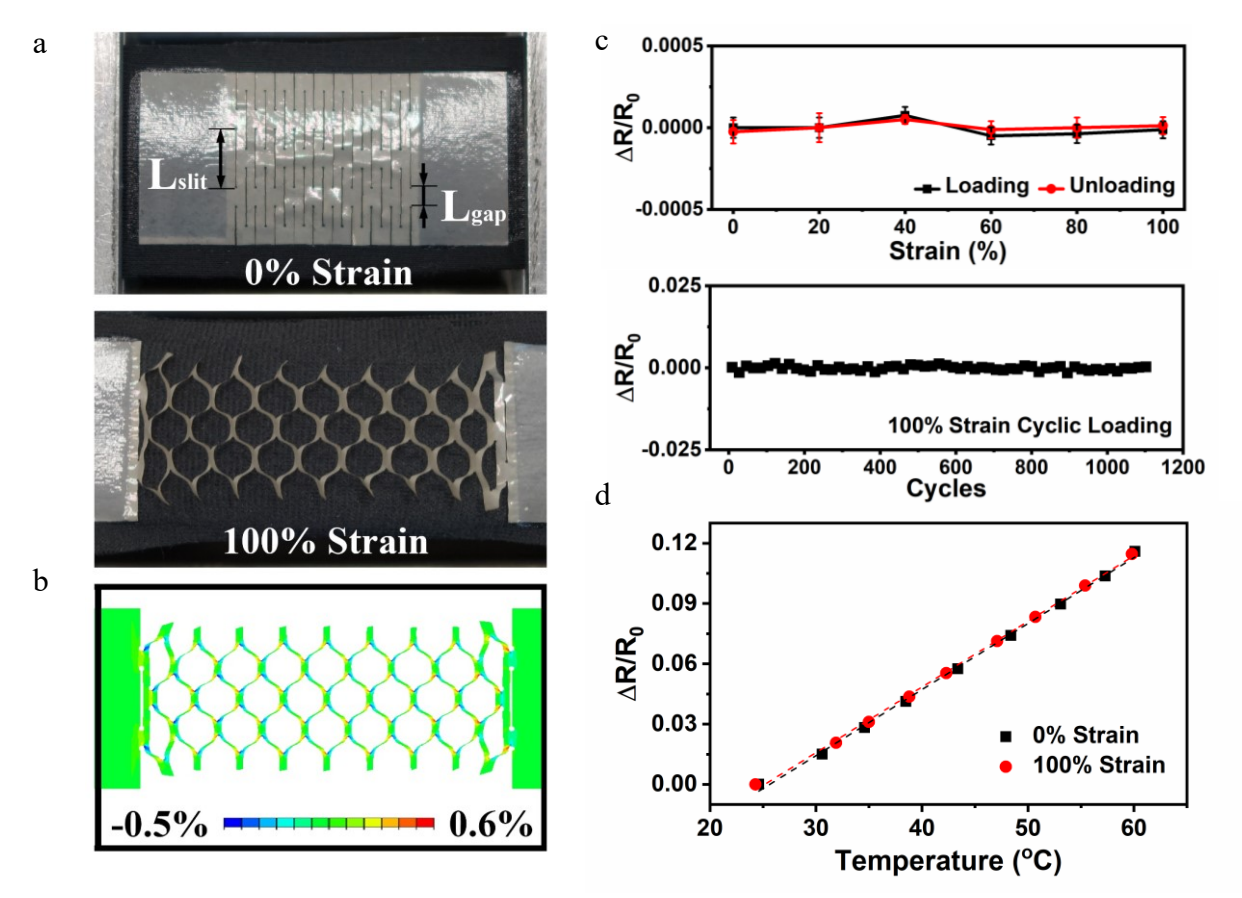


Figure 3 a) Optical images of the AgNW/PI temperature sensor at tensile strains of 0% and 100%. b) Deformed shape of the AgNW/PI temperature sensor at 100% strain from FEA simulation. c) Resistance changes of the temperature sensor under tensile quasi-static loading/unloading and dynamic cyclic loading (1100 cycles at 1 Hz). d) Resistance changes of the temperature sensor vs. temperature, characterized under 0% strain and 100% strain. Note that the initial resistance of the sensor was $145~\Omega$ at room temperature.

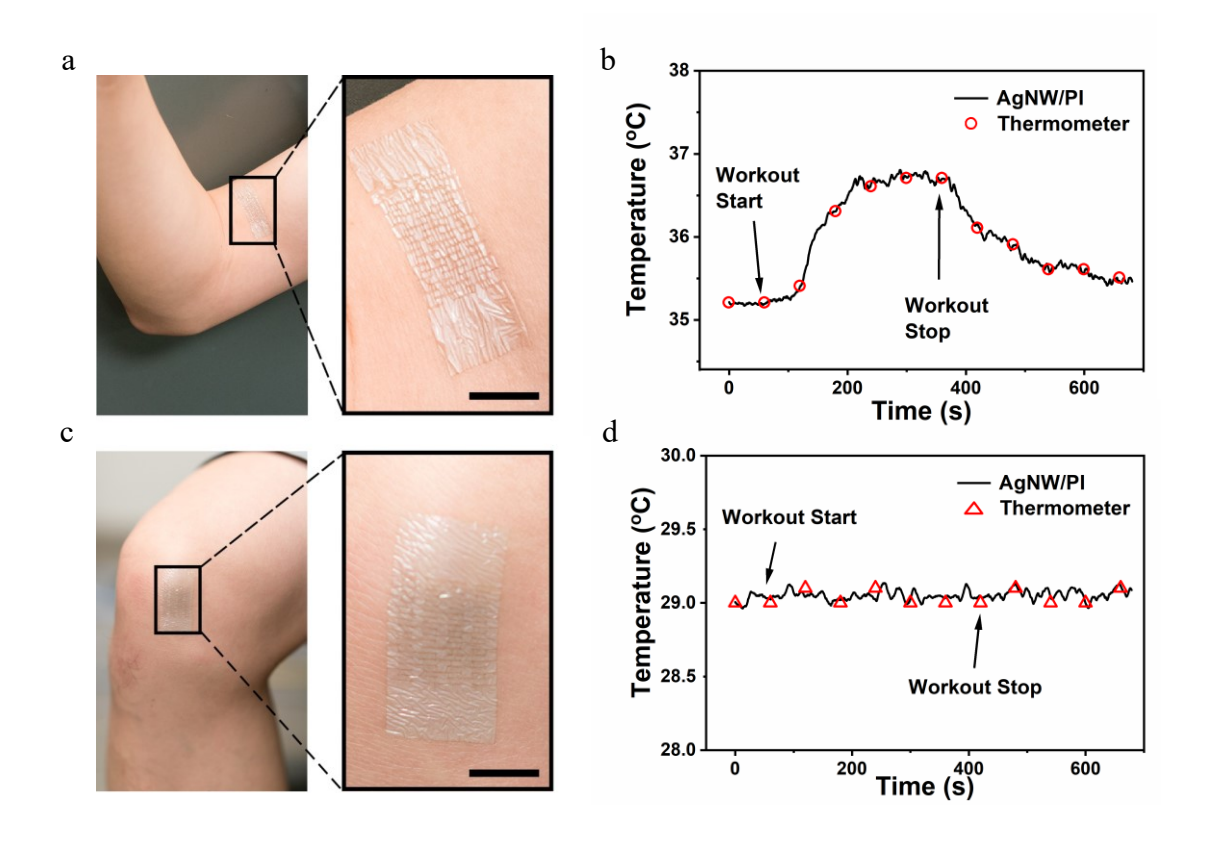


Figure 4 a) AgNW/PI temperature sensor is attached to the skin near biceps. Scale bar: 10 mm. b) Temperature recorded by the temperature sensor and infrared thermometer during biceps workout. c) AgNW/PI temperature sensor is attached to the skin near patella. Scale bar: 10 mm. d) Temperature recorded by the temperature sensor and infrared thermometer during squad workout. Note that in the images in a) and c), lead wires are not shown in the figures.

Table 1. Summary of the representative nanomaterial-enabled thermoresistive temperature sensor reported.

Materials	Sensitivity	Temperature Range	Stretchability
CNT- PEDOT:PSS ^[2]	0.61% °C ⁻¹	22 – 48 °C	
Graphene/PDMS ^[21]	0.214 °C ⁻¹	25 – 120 °C	
CNT/PET ^[24]	-0.67% °C ⁻¹	15 – 45 °C	
Si/PDMS ^[20]	0.71 Ω °C ⁻¹	25 – 110 °C	30%
Graphene/PDMS ^[22]	-1.05 % °C ⁻¹ @ 0% strain	30 - 100 °C	50%
	-2.11% °C ⁻¹ @ 50% strain		
CuNW mesh ^[25]	0.7 Ω °C ⁻¹	RT – 48 °C	80%
AgNW/PI (this work)	0.47 Ω °C ⁻¹	25 – 60 °C	100%

TOC Figure

